JMEPEG (2010) 19:1370–1379
DOI: 10.1007/s11665-010-9635-z

1059-9495/$19.00

Fabrication and Characterization of Squeezed Cast Aluminum Matrix Composites Containing Boride Reinforcements

L. Olaya-Luengas, E. Estremera-Pérez, L. Muñoz, and O.M. Suárez

(Submitted November 20, 2009; in revised form February 8, 2010)

Aluminum alloys containing 2 and 4 wt.% copper reinforced with aluminum dodecaborides were successfully fabricated by squeeze casting employing pressures up to 62 MPa. The distribution of reinforcements throughout the composites was quantified, whereas the effect of pressure on the composites density and hardness was determined. In addition, the reinforcement chemical stability was examined using high-temperature x-ray diffraction which permitted to confirm the formation of AlB_2 phase a result of AlB_{12} decomposition. The pressure effect on the squeezed composites was investigated by optical microscopy, Vickers microhardness testing, superficial Rockwell hardness testing, and differential thermal analysis. At the highest applied pressures, the castings density increased when the shrinkage porosity was practically eliminated. The composite superficial hardness improved by increasing the applied squeeze. The indirect squeeze cast technique caused Al_2Cu phase segregation to upper regions of the specimens, while conversely, the AlB_{12} reinforcements segregated preferentially at lower regions of the casting.

Keywords metal matrix composites, phase stability, squeeze casting

1. Introduction

Aluminum matrix composites (AMCs) have found extensive use in many engineering applications because of their high-specific modulus, strength, hardness and stiffness, excellent wear resistance, low thermal expansion coefficient, stability of properties at elevated temperature, reduced density, and competitive fabrication cost. The development of these materials has been driven by the aerospace and automotive industries for both nonstructural and structural applications. For instance, in recent years the aerospace community has developed high-temperature aluminum alloys capable of competing with titanium alloys (Ref 1).

The present work is focused on the fabrication via indirect squeeze casting of aluminum-copper matrix composites reinforced with AlB_{12} particles and the study of the effect of squeeze pressures on the density, microhardness, and hardness of those composites. To accomplish that goal, the distribution of AlB_{12} particles upon casting and the resulting shrinkage porosity was investigated by image analysis. Additionally, the chemical stability of those reinforcing particles was analyzed.

L. Olaya-Luengas and **E. Estremera-Pérez**, Department of Mechanical Engineering, University of Puerto Rico, Mayagüez, PR; **L. Muñoz**, Department of Chemical Engineering, University of Puerto Rico, Mayagüez, PR; and **O.M. Suárez**, Department of Engineering Science & Materials, University of Puerto Rico, Mayagüez, PR. Contact e-mail: lilia.olaya@upr.edu.

Squeeze casting is a generic term to specify a fabrication technique where solidification is promoted under high pressure within a reusable die. Squeeze casting consists of metering liquid metal into a preheated, lubricated die and forging the metal while it solidifies. The load is applied shortly after the metal begins to freeze and is maintained until the entire casting has solidified (Ref 2). Although squeeze casting is now the accepted term for this forming operation, it has also been referred to as "liquid metal forging" (Ref 2), "extrusion casting," "liquid pressing," "pressure crystallization," and "squeeze forming." Two basic methods of the process may be distinguished, depending on whether the pressure is applied directly onto the solidifying cast product via an upper or male die (punch) or the applied pressure is exerted through an intermediate feeding system: the direct and indirect squeeze casting mode (Ref 3). In indirect squeeze casting process, also the metal can be injected into the die cavity by a small diameter piston (Ref 4). For the present investigation, the indirect method was selected because it helps to eliminate porosity caused by trapped gas and solidification shrinkage.

2. Experimental Procedure

2.1 Materials Selection

Al-5 wt.% B and Al-33 wt.% Cu commercial master alloys were used to produce these AMCs. In the Al-B master alloy, boron was present forming AlB_{12} particles whereas the Al-Cu one was a binary eutectic alloy (Al-Al_2Cu).

2.2 Casting Methodology

Two sets of Al matrix composite specimens were fabricated via indirect squeeze casting with different squeeze pressures;

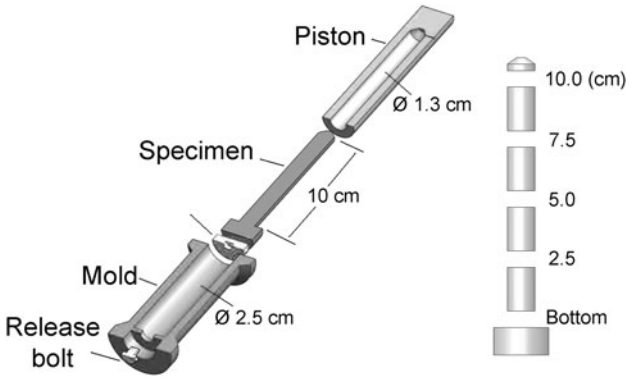

Fig. 1 Squematic cross section of the system used for squeeze casting

the specimens produced without squeeze pressure correspond to gravity casting. The first set contained 2 wt.% Cu and 4.70 wt.% B and the second set, 4 wt.% Cu and 4.40 wt.% B. In both composites, boron was present forming AlB_{12} particles, as inherited from the Al-B master alloy.

An electric furnace with a graphite crucible allowed melting the composites, which were then held at 750 °C for 30 min for the sake of homogenization. Afterward, the material was squeezed cast in an apparatus made of a stainless steel mold and a piston system shown in Fig. 1.

The stainless steel mold and hollow piston were coated with dry graphite lubricant and pre-heated in a muffle furnace at 660 °C. Afterward the molten composite matrix with solid AlB_{12} particles in suspension was poured into the stainless steel mold. Before the matrix started to solidify below 660 °C, pressure was applied with the stainless steel hollow piston during the solidification process. A hydraulic press, furbished with a special fixture fabricated to expand the piston run, applied hydrostatic pressures ranging from 0.40 to 62 MPa.

2.3 Metallographic Preparation and Microstructure Analysis

All samples were mounted in epoxy resin and then ground with a series of 320, 400, 600, 800, and 1200 grit SiC paper using water as coolant/lubricant. Polishing was carried out using 3 μm monocrystalline diamond suspension on a short felt cloth followed by final polishing with a 0.05 μm colloidal silica suspension on a short felt cloth. An inverted optical microscope and a scanning electron microscope (SEM) with a backscattered electron detector permitted characterizing the resulting microstructures.

2.4 Analysis of Volume Fraction

The volume fraction of Al_2Cu and AlB_{12} were measured from optical microscopy images using ImageJ, a public domain image analysis software (Ref 5, 6).

2.5 Bulk Density Measurements

A scale furbished with a density determination kit measured the specific gravity. Density was then calculated from specific gravity following ASTM D792-08 "Standard Test Methods for Density and Specific Gravity (Relative Density) of Plastics by Displacement," as determined by the Archimedean principle, according to Eq 1 (Ref 7).

$$\rho = \frac{W(a) \cdot \rho(fl)}{W(a) - W(fl)}, \quad \text{(Eq 1)}$$

where ρ is the density of the composite (g/cm^3); ρ(fl), density of distilled water at 23 °C (0.9976 g/cm^3); W(a), weight of the composite in air (g); and W(fl), weight of the composite in liquid, g.

2.6 Hardness Measurements

The ASTM E 384 standard test method was followed to determine the Vickers microhardness of the composites (Ref 8). A Buehler Micromet II digital microhardness tester was employed to perform the microhardness measurement on the matrix of the composite.

The superficial Rockwell hardness of these materials was performed following the ASTM E18 standard (Ref 9). The 15 T superficial Rockwell hardness test utilized a 1/16″ (1.588 mm) ball indenter and a force of 15 kgf. This method helped determine the overall effect of the microstructure (not just the matrix) on the composite mechanical behavior.

2.7 Differential Thermal Analysis

A Mettler Toledo TGA/SDTA 851^e allowed measuring the thermal evolution of the composites upon heating and cooling under a nitrogen atmosphere. The heating cycles were carried out at 10 °C/min from 25 to 750 °C, followed by a cooling cycle from 750 to 25 °C at −10 °C/min.

2.8 X-Ray Diffraction

The Rigaku Ultima III XRD with Thermo plus XRD + DSC II attachment was used to anneal the samples and analyze the diffraction pattern changes. The annealing was set to 300 °C for 2 h with heating rate 20 °C/min (max) and the diffractometer 2θ range was set from 5° to 40°.

Additionally, the composites melting process was studied using this XRD with programmable temperature controller PTC-30, set at a heating rate at 50 °C/min (max) to reach 800 °C and then holding the temperature for 2 h. The diffraction 2θ range was set from 10° to 100°. Although the XRD patterns were registered before, during and after heat treatment, in this section just patterns recorded before and after the melting tests will be shown, because the melted aluminum signal was noisy and it hid room temperature patterns. In both heat treatments, the diffractograms were recorded in situ under nitrogen atmosphere.

3. Results and Discussion

3.1 Bulk Density

Figure 2 presents the effect of the applied pressure on the composite density. The lower data points indicate that the applied pressure was not large enough to counteract the shrinkage porosity of these Al-B-based composites. Nonetheless, when these results are compared with the density of specimens fabricated using gravity casting, it becomes apparent that bulk density of the squeeze cast specimen, in general,

increased in both composite compositions. In the 2 wt.% Cu specimen, the density had a slight increment from 2.7178 to 2.7183 g/cm^3 and in the 4 wt.% Cu specimen the density raised from 2.7549 to 2.7643 g/cm^3. Although the density is expected to increase continuously with the applied pressure, Fig. 2 shows a drop in the density at 31 MPa of applied pressure.

As it is well known, when the composites are fabricated via gravity casting, shrinkage forms on the top surface and is not accounted for as a part of the internal porosity of the specimens (if both are not physically connected). With low applied squeeze pressure (0.4 and 31 MPa) during the solidification, shrinkage was not fully offset, and formed toward the mid-section of the specimens. As a result of the applied pressure (not large enough to eliminate solidification shrinkage), smaller density values were obtained.

At higher applied pressures (46 and 62 MPa), the squeezed castings density slightly increased. At these applied pressures, shrinkage porosity was practically eliminated and the density approached its theoretical value. According to the results of bulk density measured, it was reasonable to assume that pressures above 50 MPa were able to eliminate shrinkage porosity in both composites (2 and 4 wt.% Cu).

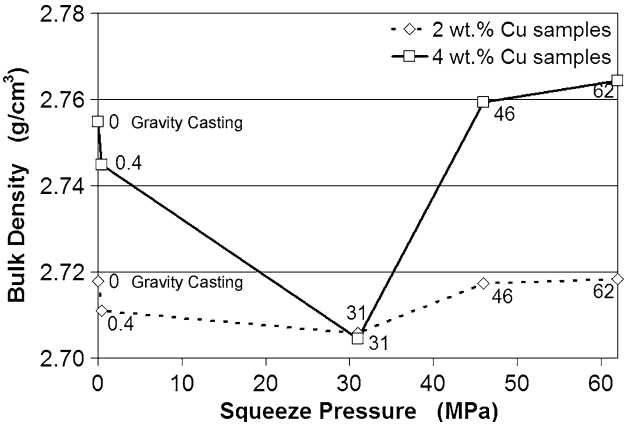

Fig. 2 Bulk density of the composites fabricated

3.2 Microstructural Characterization

Figure 3(a) presents the resulting microstructure with AlB_{12} reinforcements embedded in the aluminum matrix and Al_2Cu phase formed on the matrix grain boundaries (as part of a eutectic mixture in 4 wt.% Cu samples). Additionally, small and few particles of AlB_2 became apparent in some samples (Fig. 3b). They were preliminarily identified as diborides by comparison with a prior research on similar composites (Ref 10). Nonetheless, the apparent hexagonal shape of the particle is another indication of the nature of this diboride with hp3 crystal structure (Ref 11).

Optical microscopy also allowed observing larger segregation of the Al_2Cu phase onto the upper sections in the squeezed specimens. Figure 4(a) and (b) shows the distribution of that Al_2Cu phase at the bottom and the top sections of the same specimen.

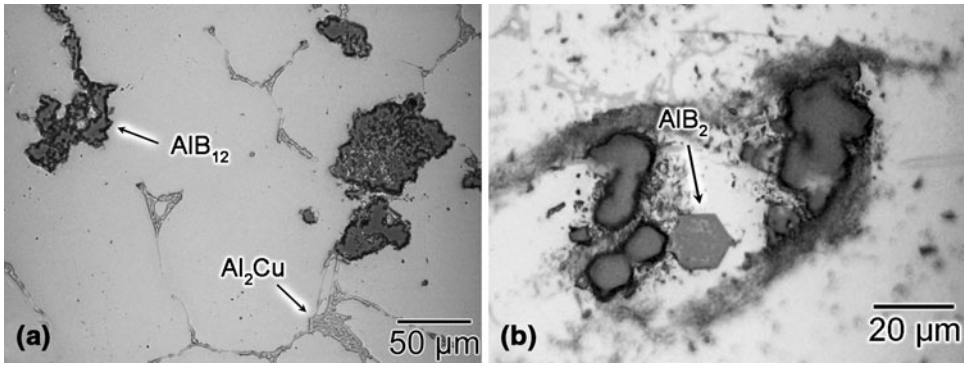

Fig. 3 Phases observed in composites. (a) 4 wt.% Cu sample fabricated with 62 MPa of squeeze pressure, cut at 10 cm of specimen bottom. (b) 4% Cu sample fabricated with 31 MPa at 5 cm of specimen bottom

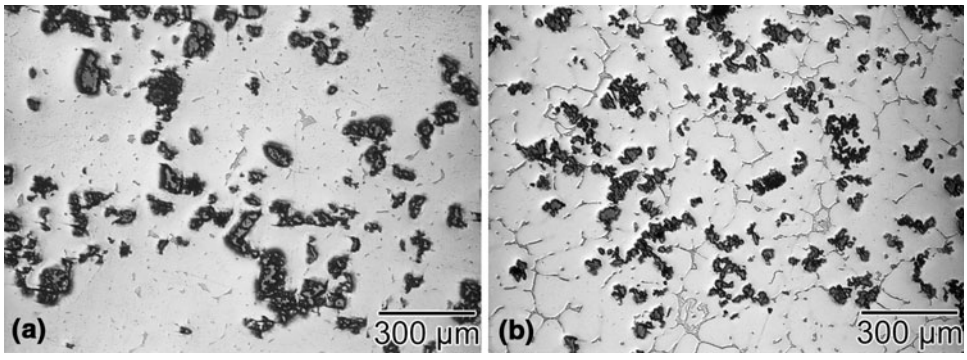

Fig. 4 Optical micrographs of the *bottom* (a) and the *top* (b) sections of the squeezed cast 4 wt.% Cu specimen fabricated with 62 MPa

As a consequence of the applied pressure, some intergranular cracks formed at mid-length of some samples. However, the cracks appeared to be stopped (or at least hindered) by the AlB_{12} reinforcements. Once more, the solidification shrinkage could not be fully offset by smaller applied squeeze pressures (0.4 and 31 MPa). Conversely, as expected, shrinkage decreased for higher applied squeeze pressures (46 and 62 MPa).

Backscattered electron imaging (BEI) allowed revealing atomic number contrast between areas with different chemical compositions, based on differences in effective atomic numbers among various regions. The phases identified initially by optical microscopy were confirmed using BEI. The effective atomic numbers (Z_{eff}) (Ref 12) calculated were 6.65 and 21.17 for AlB_{12} and Al_2Cu, respectively (Fig. 5a). BEI was used in conjunction with energy dispersive x-ray spectroscopy (EDS) to confirm the elemental composition of the AlB_{12} reinforcement, as shown in Fig. 5(b).

An overall survey of the reinforcements throughout the castings indicated that the proposed method barely improved their distribution. However, it was observed that the clustering of the borides (inherited from the fabrication of the Al-B master alloys via salt fluxes) was broken by the squeezing mechanical action. We deem this result as an improvement of the microstructure; yet, further study of the process is necessary to propose a more appealing alternative to existing in situ techniques. This microstructural analysis, however, led to the happenstance of the initial observation of the formation of small boride particles. For that reason, the bulk of this work is hereafter dedicated to the study of high-temperature XRD to throw some light on the stability of the reinforcing phase.

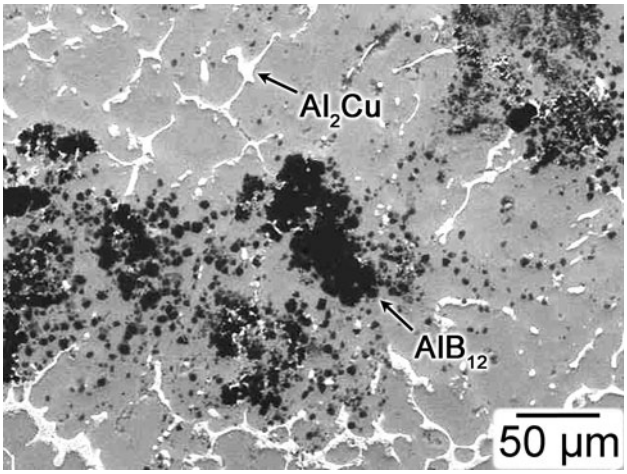

Fig. 5 BEI showing the presence of AlB_{12} and Al_2Cu

3.3 Analysis of Volume Fraction of Al_2Cu and AlB_{12} Phases

The measured volume fractions of AlB_{12} and Al_2Cu phases are presented in Fig. 6. When both 2 and 4 wt.% Cu composites were fabricated by gravity casting process (0 MPa) any segregation of AlB_{12} and Al_2Cu phases along to specimens was not detected. On the other hand, it is apparent that the squeeze casting process caused the Al_2Cu phase to form preferentially in the upper regions of the specimens. The calculated increment of this phase along the specimens (from bottom to top) was 1.5 times higher in 2 wt.% Cu samples; on the other hand, this increment was barely noticeable (only 0.2%) in the 4 wt.% Cu samples. With respect to reinforcements of AlB_{12}, these particles remained preferentially at the end regions (bottom and top) of the specimens. As well as, the specimens bottoms exposed greater amount of AlB_{12} phase compared to the mid-length of specimens, this increment was 27% and 37% for 2 and 4 wt.% Cu samples, respectively. Similarly, the specimens tops shown an AlB_{12} phase percentage increase from the mid-length of 39% and 48%.

This behavior of AlB_{12} reinforcement was likely due to the fact that the half length region the specimens had a slower cooling rate causing the reinforcement particles to displace to the lower regions during solidification. On the other hand, the upper regions were the first to solidify and its particles were retained in the matrix as in the composite fabricated via gravity casting.

3.4 Vickers Microhardness

A 25 gf load was applied for 30 s to perform the microhardness test on the aluminum matrix (free of borides and θ phase) of the composites, resulting in average values of 35.5 and 42.3 HV values for the 2 and 4 wt.% Cu squeezed samples, respectively. Moreover, the mean Vickers microhardness in gravity cast specimens was 38.5 HV for the 2 wt.% Cu specimen and 48.7 HV for the 4 wt.% Cu specimen. Evidently, Vickers microhardness of squeezed specimens was slightly lower than the measurements of the same composites fabricated via gravity casting. In both composites, the highest applied squeeze pressure (62 MPa) slightly increased the matrix

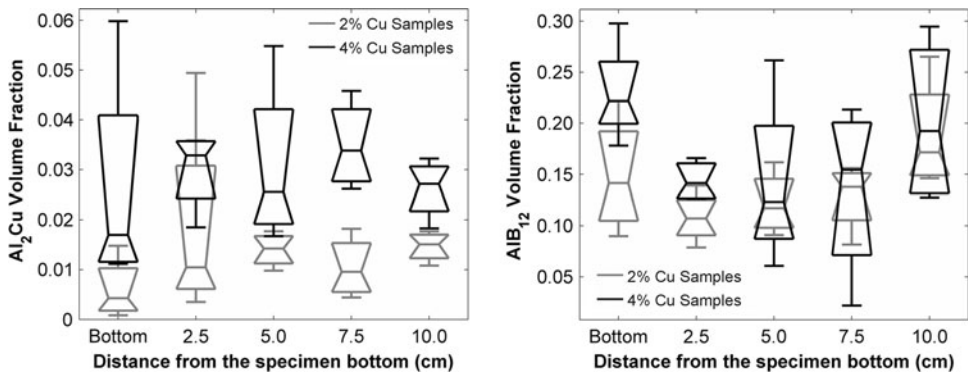

Fig. 6 Calculated volume fraction of Al_2Cu and AlB_{12} phases

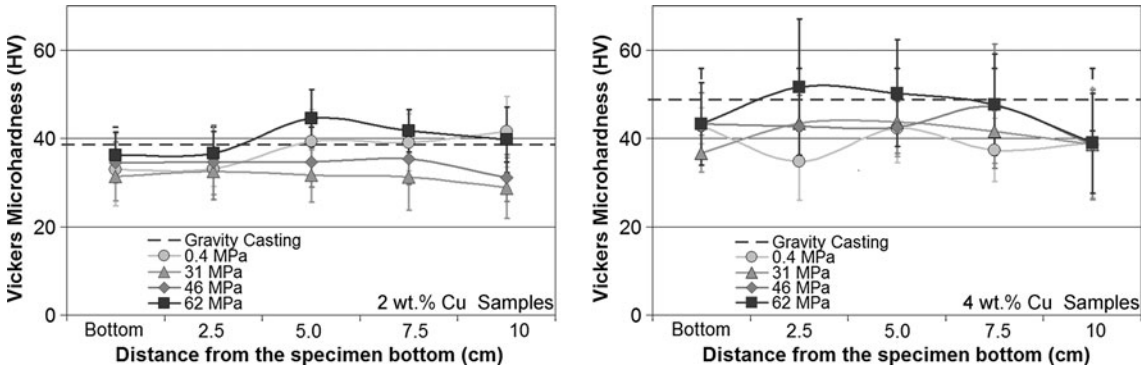

Fig. 7 Vickers microhardness (HV 25gf/30 s) values measured on the Al matrices of the AMCs fabricated with different squeeze pressures and both 2 and 4 wt.% Cu specimens

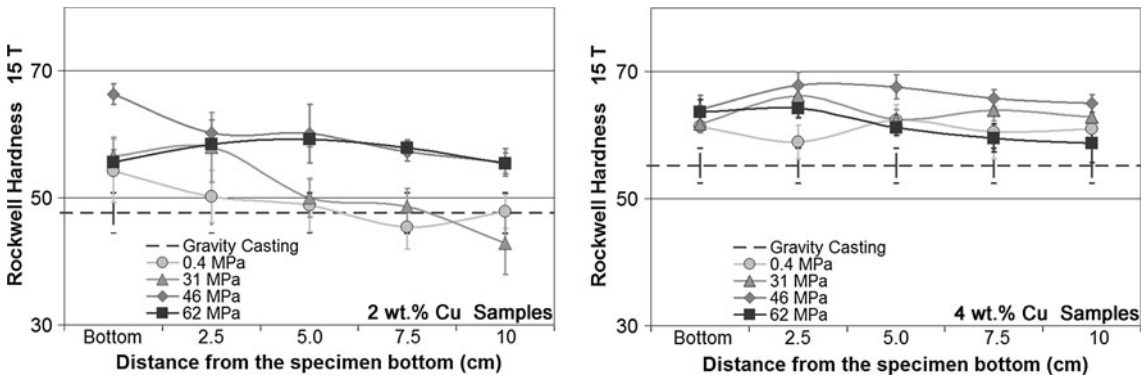

Fig. 8 Superficial Rockwell hardness (15 T) values measured on AMCs fabricated with different squeeze pressures and both 2 and 4 wt.% Cu specimens

hardness, as observed in Fig. 7. Nonetheless, for the highest squeeze pressures (46 and 62 MPa) the average microhardness was equal to that measured on the gravity cast specimens.

3.5 15 T Superficial Rockwell Hardness

Figure 8 shows superficial Rockwell hardness of composites fabricated via squeeze casting and gravity casting as a function of the distance along the specimens. In Fig. 8, the 4 wt.% Cu squeezed specimens showed higher superficial hardness than the 2 wt.% Cu squeezed specimens with 63 HR15T. This evinces the hardening effect caused by the higher concentration of copper. As mentioned before, the higher pressure induced that the reinforcements be redistributed throughout the specimen. Seemingly, these differences in distribution caused a nonhomogeneous composite material with some superficial hardness variations.

Evidently, the superficial Rockwell hardness was improved with the implementation of squeeze casting as a fabrication method. In the first set of 2 wt.% Cu specimens, the superficial hardness increased 14.4% and in the second set of 4 wt.% Cu specimens the increment was 14%, in both cases with respect to superficial hardness of gravity cast samples. This behavior showed that the superficial hardness was affected by applied squeeze pressure. Likely, this is due to the enhanced solubility of Cu and the decreasing of shrinkage porosity by the applied pressures.

3.6 Differential Thermal Analysis

During the heating cycle the differential thermal analysis (DTA) curves exhibited two endothermic peaks. The first peak (at lower temperature) corresponded to an apparent *eutectic* reaction (solidus line) and the second one to the Al matrix melting point (liquidus line). It is evident that these temperatures do not correlate exactly with those in the binary Al-Cu phase diagram in Fig. 9.

This apparent lack of correlation is caused by the overall copper percent in the composites is slightly lower than the copper levels in only matrix in the same composites. These small differences in copper mass balancing are reflected as a displacement to the right in the composition axes from 4 to 4.22 and from 2 to 2.11 wt.% copper (Fig. 9). Other way to interpret these copper differences is by assuming that the phase diagram is shift to the right as the arrow shown in Fig. 9.

In order to corroborate this shifting, a set of DTA experiments were conducted. The thermal event due to the first reaction upon heating was only observed in the 4 wt.% specimens at 542 ± 1.2 °C (Fig. 10). This temperature was similar in all samples and represents the eutectic reaction (solidus line): $\alpha Al + \theta \rightarrow$ liquid. Additionally, this reaction was confirmed in the microstructure analysis of these samples, through the corresponding micrographs the eutectic Al_2Cu phases were identified at the grain boundaries of the matrix (Fig. 11). This recorded temperature was slightly lower than

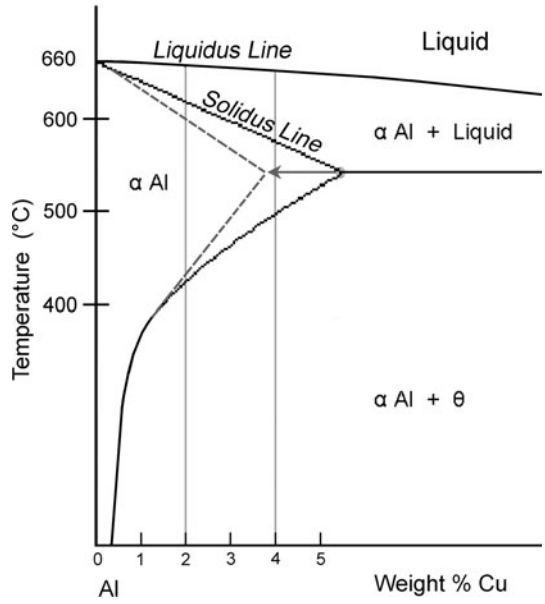

Fig. 9 Phase diagram Al-Cu

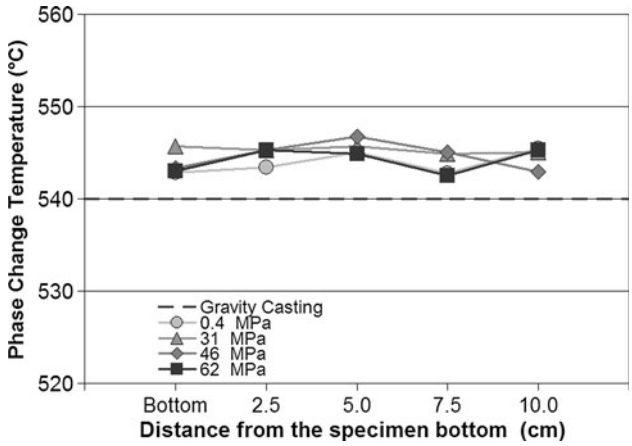

Fig. 10 Measured temperatures in the 4% Cu samples

eutectic temperature of the Al-Cu phase diagram, i.e., 548 °C. Subsequently, this behavior confirmed again that the Al-Cu phase diagram of this matrix reinforced with borides shifted to the left, as shown the dotted lines in Fig. 9. In other words, the maximum solubility of Cu in αAl (at 548 °C in Fig. 9) was reduced to a concentration between 2 and 4 wt.% Cu. Table 1 shows the differences between the obtained temperatures in the DTA (heating and cooling) and from the literature.

As mentioned, the Al_2Cu or θ phase formed preferentially on the top regions of the specimens. Consequently, the melting points of the samples tops were shifted to the left in the DTA curves (lower temperature). Figure 12 shows the tendency described previously for a specimen fabricated with 46 MPa of squeeze pressure. The first derivative plots were used to confirm the thermal events (melting points or other phase changes).

The highest squeeze pressures (31, 46, and 62 MPa) increased the melting points in the bottom regions of all specimens, as shown in the DTA curves in Fig. 13. According

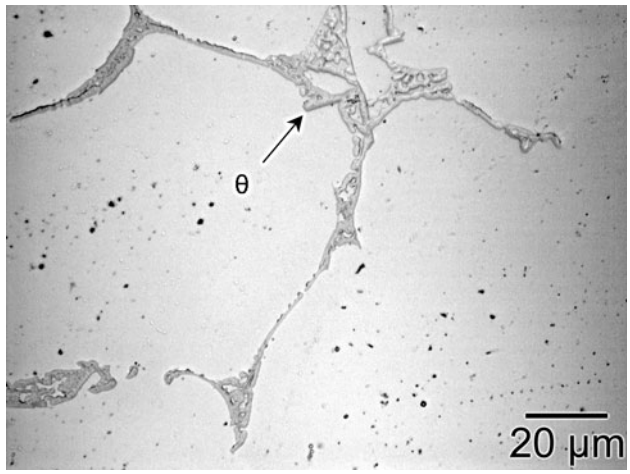

Fig. 11 Al-Al_2Cu eutectic observed in the matrix grain boundaries of 4 wt.% Cu samples

Table 1 Comparative chart of phase change signal (upon heating and cooling) and solidus line from phase diagram

Wt.% Cu in the matrix	Phase change (solidus line) upon heating (DTA onset), °C	Phase change (solidus line) upon cooling (DTA onset), °C	Eutectic temperature (solidus line) (Ref 17), (°C)
4.22	542	541	548

to the Al-Cu phase diagram, that behavior indicates Al-richer matrix in the bottom regions of both specimens. The melting reactions (DTA onset) were 648 ± 3 °C for the 2 wt.% Cu specimens and 639 ± 3 °C for the 4 wt.% Cu specimens. These temperatures were slightly lower than expected according to those in the Al-Cu phase diagram (Table 2).

The average melting points of the matrix of the squeezed specimens were clearly higher than the melting points of the specimens fabricated via gravity casting. This relative increment was 0.5 and 1.4% for 2 and 4% Cu specimens, respectively. In addition, in Fig. 13 there is a perceptible slope between the bottoms and the rest of the squeezed specimens. This slope is equivalent to a melting point increment of 6.2 and 6.4 °C for the 2 and 4 wt.% Cu samples, respectively, from the bottom to the rest of specimens.

3.7 X-Ray Diffraction

3.7.1 XRD + Differential Scanning Calorimeter. In order to confirm the sensitivity of the XRD instrument with the differential scanning calorimeter (DSC) attachment, the aluminum diffraction angle in the set range is 2θ = 38.474° for the (111) plane (Ref 13). This peak was compared for the five distances along each specimen. According to Fig. 14, during heat treatment, this aluminum peak shifted to the left. This behavior corroborated the thermal expansion of the aluminum unit cell in agreement with Bragg's law. When the samples were cooled to room temperature after annealing, the aluminum peak returned to its original position.

The composite matrix (a solid solution of Cu in αAl) contained also Al_2Cu, observed by optical microscopy and detected by the XRD. The Al_2Cu diffraction peaks within the

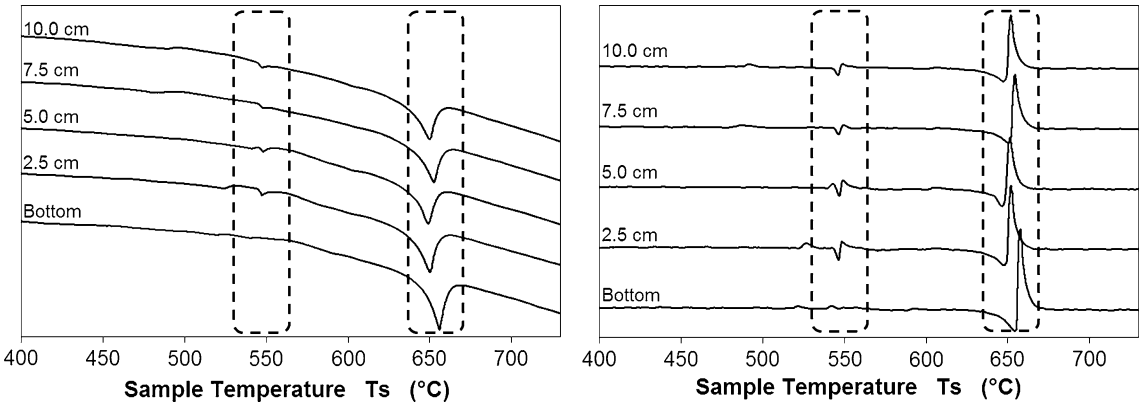

Fig. 12 DTA and first derivative curves of 4 wt.% specimen fabricated with 46 MPa of squeeze pressure

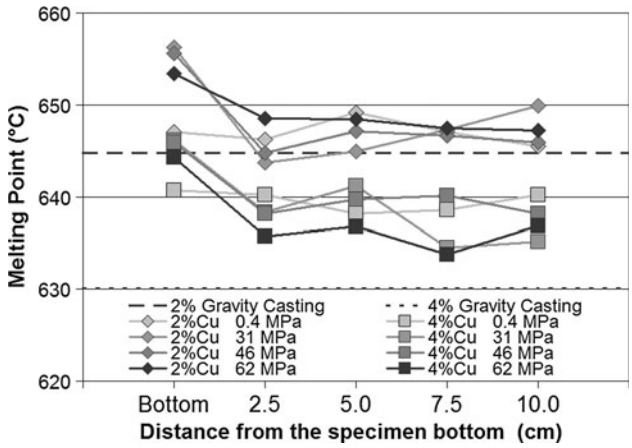

Fig. 13 Melting points of all analyzed samples

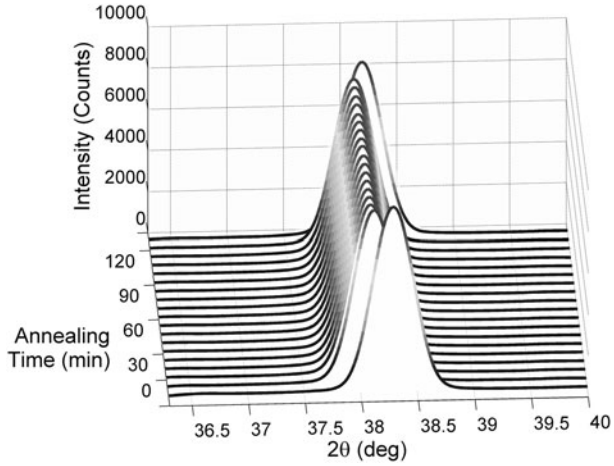

Fig. 14 XRD pattern of Al 2θ = 38.4° measured at 5 cm from specimen bottom. 2 wt.% Cu sample fabricated by squeeze casting with 31 MPa of applied pressure

Table 2 Comparative chart of melting point, solidification, and liquidus line of reference

Wt.% Cu in the matrix	Melting point upon heating (DTA onset), °C	Solidification upon cooling (DTA onset), °C	Melting point (liquidus line), °C (Ref 17)
2.10	648	654	655
4.22	639	649	650

2θ = 5°-40° range were 20.620° (110), 29.386° (200), and 37.867° (211) (Ref 14). Figure 15 shows the first Al_2Cu peak detected with increasing heights during heat treatment. The third Al_2Cu peak at 2θ = 37.867° was not evident, as this peak overlapped with the aluminum peak at θ = 38.474° (111). The amount of Al_2Cu increased during the annealing heat treatment due to further stabilization of the microstructure regardless of the presence of the borides. In effect, more Cu atoms from the Al solid solution precipitated forming more θ phase. This was corroborated during the XRD + DSC experiments.

According to the literature (Ref 15), there are three reported AlB_{12} peaks from 2θ = 5° to 40° with relative intensity higher

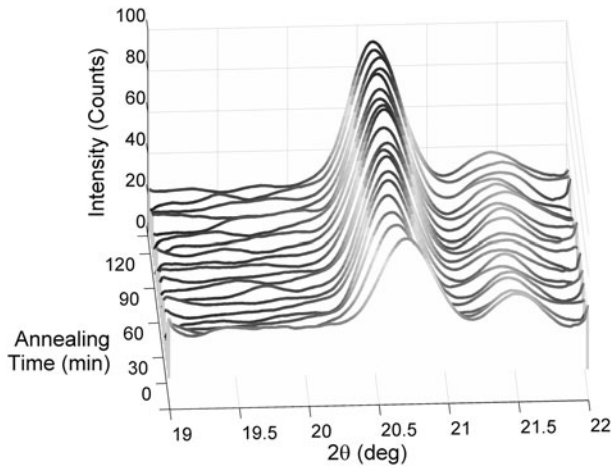

Fig. 15 Al_2Cu peak increasing 2θ = 20.6° at 10 cm from specimen bottom. 2 wt.% Cu sample fabricated by squeeze casting with 31 MPa of applied pressure

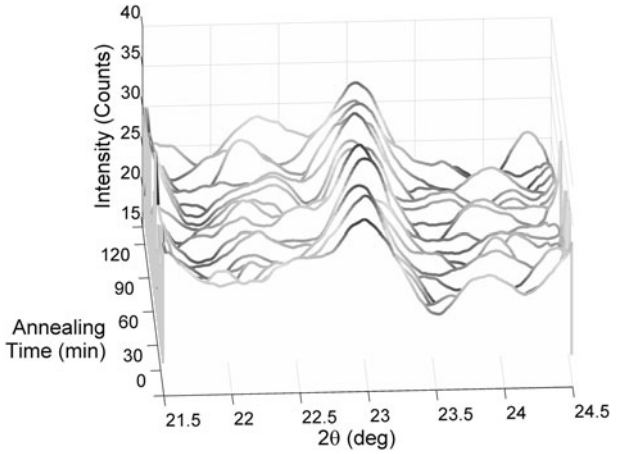

Fig. 16 AlB_{12} peak decreasing 2θ = 22.6° at specimen bottom. 4 wt.% Cu sample fabricated by squeeze casting with 31 MPa of applied pressure

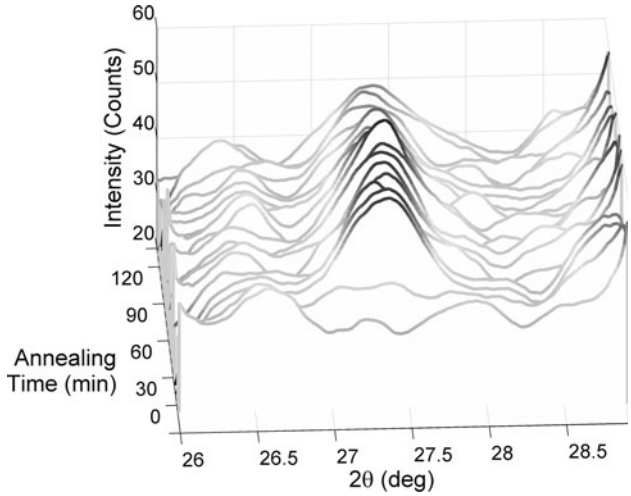

Fig. 17 AlB_2 peak increasing 2θ = 27.4° at 2.5 cm from specimen bottom. 2 wt.% Cu sample and 31 MPa of squeeze pressure

than 25%: 22.607° (202), 36.496° (242), and 36.947° (341) all detected during this experiment using the XRD + DSC. Figure 16 shows the first AlB_{12} peak detected at 2θ = 22.607°; this peak height decreased during annealing. The second and third AlB_{12} peaks at 2θ = 36.497° and 36.947° were also detected as one wide peak. A slight shift to the left during heat treatment observed can be interpreted by unit cell expansion; upon cooling the peak and returned to the original 2θ position. Also, during the heat treatment, the intensity of this wide peak decreased slightly.

As aforementioned, some AlB_2 particles were previously detected via optical microscopy and SEM. This phase was detected in the diffractograms recorded at 300 °C in the XRD + DSC. According to the literature (Ref 11), there are two AlB_2 peaks within the 2θ = 5-40° range: at 2θ = 27.418° (001) and 34.414° (100). The observed AlB_2 peak at θ = 27.418° presented a noticeable intensity increase upon annealing in all samples. Before annealing, none of the samples showed this 27.418° AlB_2 peak. Figure 17 depicts the AlB_2 peak behavior described. The AlB_2 peak at 2θ = 34.414° increased slightly in both 2 and 4 wt.% Cu specimens during heat treatment. This could be readily interpreted as an increasing formation of AlB_2 phase in both 2 and 4 wt.% Cu specimens during annealing due to the destabilization of the AlB_{12} phase.

This formation of AlB_2 due to the chemical instability of AlB_{12} particles is proved by the slight reduction of AlB_{12} peak heights at 2θ = 36.496° and 36.947° and the appearance and heightening of AlB_2 peaks during heat treatment.

3.7.2 High-Temperature XRD. According to the literature (Ref 13, 16), there are six aluminum peaks for the 2θ range studied 38.474° (111), 44.723° (200), 65.100° (220), 78.234° (311), 82.441° (222), and 99.190° (400). All these peaks were identified by XRD. Figure 18 shows a XRD pattern from 2θ = 10° to 100° of a squeezed sample before and after heat treatment. After melting the samples at 800 °C in XRD, the intensity of aluminum peaks decreased except for the peak at 2θ = 82.4.

The Al_2Cu phase was also detected in these diffractograms at 2θ = 20.620° (110), 29.386° (200), 42.591° (112), 47.332° (310), 47.808° (202), and 97.062° (314) (Ref 14). The first Al_2Cu peak had an important increment, but the other peaks tended to keep the same intensity (Fig. 19).

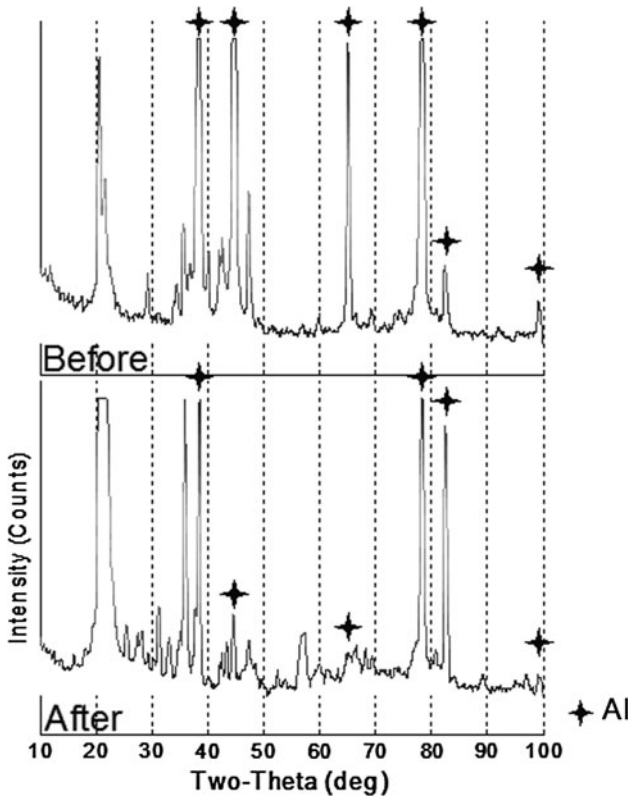

Fig. 18 XRD Al patterns of cross section at 5 cm from bottom specimen fabricated with 4 wt.% Cu and 31 MPa of squeeze pressure

Upon melting, it was very important to study the reinforcement behavior in the composites. The AlB_{12} was detected by XRD analysis, at 2θ = 22.607° (202) and 36.947° (341) (Ref 15). The first AlB_{12} peak was not readily observable as this peak overlaps with the Al_2Cu peak. However, the AlB_{12} peaks tended to hold the same intensity in both specimens (Fig. 20).

AlB_2 detection by optical microscopy and SEM motivated further scrutiny of the AlB_2 peaks using high-temperature

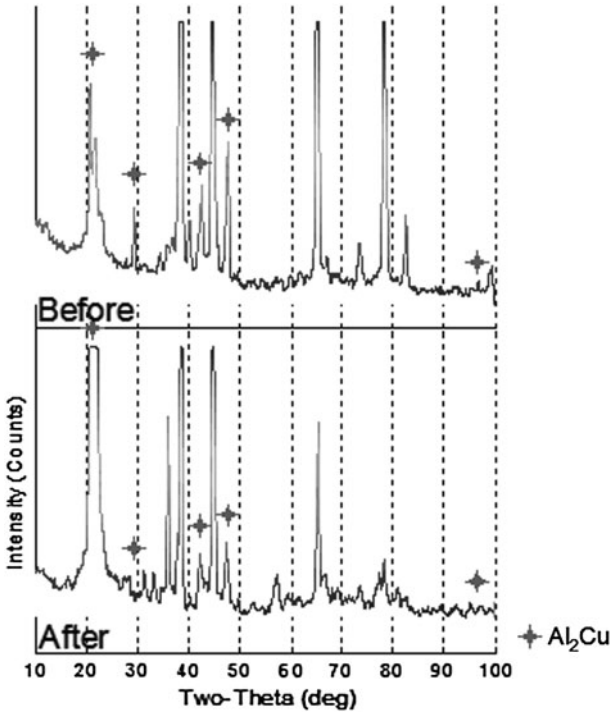

Fig. 19 XRD Al_2Cu patterns of cross section at 10 cm from bottom specimen fabricated with 4 wt.% Cu and 31 MPa of squeeze pressure

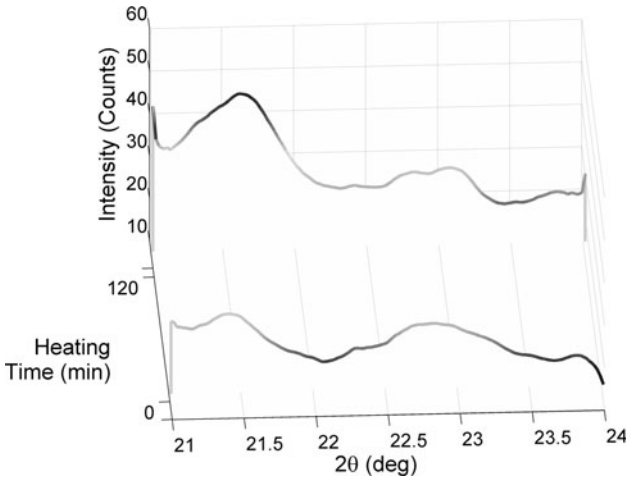

Fig. 20 AlB_{12} peak decreasing $2\theta = 22.6$ at specimen bottom. Smelted sample at 800 °C hold 2 h. 4 wt.% Cu and 0.4 MPa of squeeze pressure

XRD. According to the literature (Ref 11), there are four peaks with their intensity higher than 25%: $2\theta = 34.414°$ (100), 44.542° (101), 56.539° (002), and 61.694° (110). The first AlB_2 peak decreased slightly, while the remaining peaks showed that their intensity increased, as shown in Fig. 21. One more time the AlB_2 phase increment was detected by XRD tests confirming that the formation of AlB_2 caused by the decomposition of AlB_{12} particles, in this case during melting of the matrix.

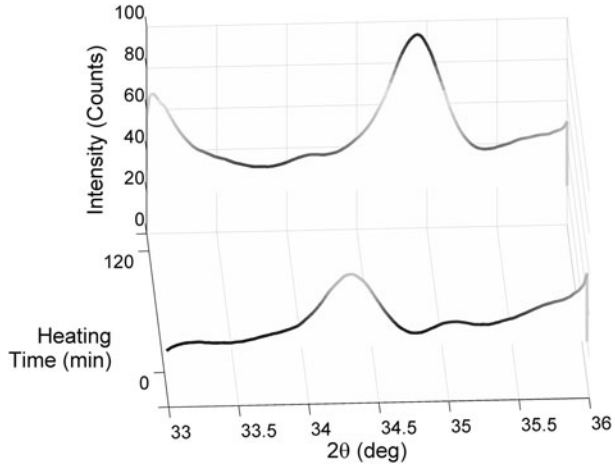

Fig. 21 AlB_2 peak increasing $2\theta = 34.4°$ at 2.5 cm from specimen bottom. Smelted sample at 800 °C hold 2 h. 2 wt.% Cu and 0.4 MPa of squeeze pressure

4. Conclusions

As a result of the squeeze casting process, the Al-Cu-B composites studied possessed better microstructural characteristics compared with conventionally cast ones. A key factor was the control of the applied pressure. Effects of this parameter on the density, microhardness, and superficial hardness of AlB_{12}/Al composites were investigated in this work.

The bulk density had a slight increase due to the highest applied pressure (from 0 to 62 MPa) during squeeze casting. This density increment proved that the composites experimented a shrinkage porosity reduction, which was also corroborated via optical microscopy.

In both composites, the highest applied squeeze pressure (62 MPa) appeared to slightly increase the matrix hardness. In general, the average matrix hardness of squeezed specimens was slightly lower than the measurements of the same composites fabricated via gravity casting (0 MPa). Only for the highest squeeze pressures (46 and 62 MPa), the mean matrix microhardness was equal to gravity casting specimens.

Superficial Rockwell hardness was improved with the implementation of squeeze casting as a fabrication method than gravity casting specimens. In the 2 wt.% Cu composites, the superficial hardness increased 14.4% and in the second set of 4 wt.% Cu specimens the increment was 14%. The squeeze pressure caused that the matrix were compacted originating denser composites.

The DTA experiments allowed detecting the eutectic reaction $(\alpha Al + \theta \rightleftarrows \text{Liquid})$ in the 4 wt.% Cu specimens fabricated by squeeze casting. The presence of the θ eutectic phase was corroborated by optical microscopy and XRD. As consequence, we proposed an extension of the eutectic line to lower amounts of Cu in Al-Cu phase diagram when AlB_{12} particles are present. Furthermore, the segregation of Al_2Cu phase to upper regions was ratified by this technique; the Al melting temperatures in the bottom regions was higher than the rest of specimens indicating Al-richer matrices.

By means of XRD + DSC larger amounts of Al_2Cu (θ) were observed during the annealing of samples due to further stabilization of the microstructure regardless of the presence of

borides. The formation of AlB_2 as a result of AlB_{12} decomposition was proved by XRD + DSC experiments. Similar results were obtained from the high-temperature XRD, where the AlB_{12} phase was slightly reduced and the AlB_2 phase was increased. As consequence, we confirmed the presence of both types of reinforcements in the composites fabricated via squeeze casting and the lack of chemical stability of AlB_{12} for the composite fabrication conditions.

Acknowledgments

This work was supported by the National Science Foundation through grants no. DMR 0351449 (PREM Program), no. HRD 0833112 (CREST Program), and no. CBET 0619349 (MRI Program). The authors would to like thank to KB Alloys for the donation of the Al-B master alloys, and to express their deep gratitude to Professors Paul Sundaram and Jayanta Banerjee (University of Puerto Rico—Mayagüez) for reading and refining this manuscript.

References

1. M. Arhami, F. Sarioglu, A. Kalkanli, and M. Hashemipour, Microstructural Characterization of Squeeze-Cast Al-8Fe-1.4V-8Si, *Mater. Sci. Eng. A*, 2007, **485**, p 218–223
2. J.L. Dorcic and S.K. Verma, Squeeze Casting, *ASM Handbook*, Vol 15: Casting, 9th ed, ASM International, Materials Park, OH, 1988, p 323–327
3. M.R. Ghomashchi and A. Vikhrov, Squeeze Casting: An Overview, *J. Mater. Proc. Technol.*, 2000, **101**, p 1–9
4. Z.W.-W. Zhang Ming and H.-d. Zhao, Effect of Pressure on Microstructures and Mechanical Properties of Al-Cu-Based Alloy Prepared by Squeeze Casting, *Trans. Nonferrous Metal Soc. China*, 2007, **17**, p 496–501
5. E.E. Underwood, Quantitative Metallography, Metallography and Microstructures, *ASM Handbook*, Vol 9: Metallography and Microstructures, 9th ed, ASM International, Materials Park, OH, 1985, p 123–134
6. H. Baker, Ed., ASM, Introduction to Alloy Phase Diagram, *ASM Handbook*, Vol 3: Alloy Phase Diagrams, 10th ed, ASM International, Materials Park, OH, 1992, p 1.7–1.29
7. Sartorius, *Sartorius User's Manual Density Determination Kit Sartorious AG*, Sartorius, Goettingen, Germany, 2004
8. "Test Method for Microindentation Hardness of Materials," E 384-07, *Annual Book of ASTM Standards*, ASTM, p 1–33
9. "Test Methods for Rockwell Hardness of Metallic Materials," E 18-07, *Annual Book of ASTM Standards*, ASTM, p 1–36
10. O.M. Suárez, J. Yupa Luna, and H.E. Calderón, Precipitation Hardening in Novel Cast Aluminum Matrix Composite, *AFS Transaction 2003*, American Foundry Society, Des Plaines, IL, 03-058(02), p 159–166
11. W. Wong-Ng, H. McMurdie, B. Paretzkin, C. Hubbard, and A. Dragoo, NBS (USA). ICDD Grant-in-Aid, 1988
12. S. Jayaraman and L.H. Lanzl, *Clinical Radiotherapy Physics*, Vol I, 2nd ed, Springer, Berlin, Germany, 2004, p 87
13. H.E. Swanson and E. Tatge, Standard X-Ray Diffraction Powder Patterns, *Nat. Bur. Stand. (U.S.)*, 1953, **I**, p 11
14. E.E. Havinga, H. Damsma, and P. Hokkeling, Compounds and Pseudo-Binary Alloys with the $CuAl_2$(C16)-Type Structure I. Preparation and X-Ray Results, *J. Less Common. Met.*, 1972, **27**(2), p 169–186
15. J.A. Kohn and D.W. Eckart, Aluminum Boride, AlB_{12}, *Anal. Chem.*, 1960, **32**(2), p 296–298
16. R.W.G. Wyckoff, Cubic Closest Packed, ccp, Structure, *Cryst. Struct.*, 1963, **1**, p 7–83
17. University of Cambridge, *Al-Cu Phase Diagram*, 2009 (cited; available from: http://www.doitpoms.ac.uk/miclib/pds.swf?targetFrame=Al-Cu)